

BBN And CMB Constraints On Dark Energy

James P. Kneller

Department of Physics, The Ohio State University, Columbus, OH 43210
*Department of Physics, North Carolina State University, Raleigh, NC 27695-8202 **

Gary Steigman

Department of Physics, The Ohio State University, Columbus, OH 43210 †
Department of Astronomy, The Ohio State University, Columbus, OH 43210

(Dated: September 14, 2018)

Current observational data favor cosmological models which differ from the standard model due to the presence of some form of dark energy and, perhaps, by additional contributions to the more familiar dark matter. Primordial nucleosynthesis provides a window on the very early evolution of the universe and constraints from Big Bang Nucleosynthesis (BBN) can bound the parameters of models for dark matter/energy at redshifts of order ten billion. The spectrum of temperature fluctuations imprinted on the Cosmic Microwave Background (CMB) radiation opens a completely different window on the universe at epochs from redshifts of order ten thousand to nearly the present. The CMB anisotropy spectrum provides constraints on new physics which are independent of, and complementary to those from BBN. Here we consider three classes of models for the dark matter/energy: extra particles which were relativistic during the early evolution of the universe (“ X ”); Quintessence models involving a minimally-coupled scalar field (“ Q ”); models with a non-minimally coupled scalar field which modify the strength of gravity during the early evolution of the universe (“ G ”). We constrain the parameters of these models using data from BBN and the CMB and identify the allowed regions in their parameter spaces consistent with the more demanding joint BBN and CMB constraints. For “ X ” and “ Q ” such consistency is relatively easy to find; it is more difficult for the “ G ” models with an inverse power law potential for the scalar field.

I. INTRODUCTION

Current and ongoing space-based and ground-based observational programs have provided increasingly precise data enabling us to view the present and recent universe with hitherto unprecedented clarity and detail. These data have led to a current “standard” model of cosmology in which “dark matter” and “dark energy” of unknown origins play significant roles. At the same time, the earlier, radiation dominated (RD) evolution of the universe remains largely hidden from view. These early epochs, which may harbor valuable clues to the nature of the dark matter/energy are shrouded by the huge optical depth of the pre-recombination plasma. As a result, they can only be explored indirectly, through the comparisons with observations of the predictions of primordial nucleosynthesis (“big bang nucleosynthesis”: BBN) and of the temperature fluctuations in the spectrum of the cosmic microwave background radiation (CMB). Studies of BBN and the CMB offer a valuable complement to probes of the recent structure and evolution of the universe and, in conjunction with them, may provide unique constraints on competing models for the dark energy. For example, although the abundances of the light elements produced during BBN depend largely on the universal density of baryons, they are also sensitive to the early universe expansion rate which, in turn, is determined by the energy

density in relativistic particles and, on the strength of gravity. Thus, BBN can not only constrain the contribution of additional energy density beyond that predicted for the standard model of particle physics, it can also probe the strength of the gravitational interaction during such early epochs. Similarly, the CMB fluctuation spectrum depends not only on the total energy density and the magnitude of its relativistic component, but also on the expansion rate and the strength of gravity. As a result, BBN and the CMB have the potential to distinguish among – or at least constrain – competing models for the dark energy some of which leave the strength of the gravity invariant while adding to the energy density, while others may modify both.

In this paper we compare and contrast the modifications to the standard model BBN and CMB predictions in the presence of extra, relativistic energy (“equivalent neutrinos”), for those models of “Quintessence” which, during RD epochs, contribute a fixed fraction of the relativistic energy density, and for non-minimally coupled scalar fields (one of whose effects is to alter the strength of the gravitational constant G). After an introduction to, and an overview of the non-standard cosmologies explored here (§II), the BBN predictions for these three general models are compared and contrasted and current data is employed to provide constraints on them in §III. In §IV an overview is provided of the physical origin of the CMB fluctuations in the standard model as a prelude to our discussion of the predictions in the non-standard cosmologies (§V). The CMB constraints are presented in §VI and in §VII they are combined with those from BBN to provide joint constraints on the non-standard cosmolo-

*current address

†mailing address

gies considered here. Our results on the joint BBN-CMB constraints are summarized in §VIII. Unless otherwise stated, we use units in which $\hbar = c = 8\pi G = 1$.

II. NON-STANDARD COSMOLOGIES

Before we begin discussing the implications for BBN and the CMB of the “new physics” we are considering it is worth spending some time investigating the effects of each upon cosmology in general. As a reference we take the standard model to be geometrically flat, containing three, light neutrinos, baryons along with cold dark matter (CDM), and a cosmological constant (Λ). For numerical estimates we will often adopt the so-called concordance values for the density parameters: $\Omega_M = 0.3$, $\Omega_\Lambda = 1 - \Omega_M = 0.7$, and for the present value of the Hubble parameter: $H_0 = 72 \text{ kms}^{-1}\text{Mpc}^{-1}$.

“X”

In many extensions of the standard models of cosmology and of particle physics there can be “extra” energy density contained in new particles or fields, ρ_X . Adding energy always results in an increase of the expansion rate, H , at a given redshift since

$$H^2 = \frac{\rho}{3} \quad (1)$$

where ρ is the total energy density. The increased expansion rate in turn implies that the age of the Universe at a given scale factor,

$$t(a) = \int_0^a \frac{1}{aH} da \quad (2)$$

is younger than in the standard model. If the stress energy tensor for X is conserved then the rate of change of the energy density for X obeys

$$\dot{\rho}_X + 3H(\rho_X + P_X) = 0 \quad (3)$$

where the dot denotes the derivative with respect to cosmic time and P_X the pressure. The equation of state, $w_X = P_X/\rho_X$, is therefore all that is required to determine the evolution of ρ_X .

When X behaves like radiation, that is when $w_X = 1/3$, this additional energy density varies with the scale factor, a , as $\rho_X \propto a^{-4}$. In the remainder of this paper we shall assume this behavior for “X”. Of course, other equations of state are possible, leading to different scalings of the X-density with a but, because this evolution of ρ_X for $w_X = 1/3$ is exactly the same as that for the photon and neutrino energy densities [75] extra relativistic energy is a simple extension of the standard model.

“Q”

Another example of “new physics” is the positing of a Quintessence field to replace the cosmological constant as a source of the dark energy in the standard model [1]. Quintessence has become an increasingly attractive alternative to Λ because, by making the dark energy dynamic, it helps alleviate the large discrepancy between the matter/radiation and vacuum energy densities most apparent during the early Universe. Virtually all Quintessence models are taken to be a minimally-coupled scalar field ϕ with an energy density $\rho_Q = \dot{\phi}^2/2 + V(\phi)$ and a pressure $P_Q = \dot{\phi}^2/2 - V(\phi)$ where $V(\phi)$ is the potential energy. If the field only interacts with the other constituents of the cosmic fluid gravitationally then equation (3) also applies to ρ_Q but the characteristic of Quintessence is a non-trivial equation of state that is not known a priori. However by substituting the expression for ρ_Q and P_Q into equation (3) we obtain the Klein-Gordon equation for ϕ

$$\ddot{\phi} + 3H\dot{\phi} + V_\phi = 0 \quad (4)$$

where $V_\phi \equiv dV/d\phi$. Here, once $V(\phi)$ is specified, there are no unknown functions. For many potentials there exist solutions to this equation to which the field converges from a wide range of initial conditions. Solutions of this type are generically dubbed “tracker” solutions even though this term was originally introduced to distinguish a specific class of models [1]. We shall assume that the field has reached this tracker solution long before BBN. The evolution of the field is controlled by the form of the potential and there are many different models in the literature from which to choose. This is unfortunate because there is then no generic behavior or consequence of a dynamic dark energy except that we may state that if the Quintessence equation of state w_Q is ever larger than -1 , then the total energy density at a given redshift will be larger than in the standard model. If we restrict ourselves to tracker potentials then, very roughly, we may divide them into those where the Quintessence energy density during the radiation dominated epoch is significant and those where it is not. Examples of the latter type include the popular Inverse Power Law potentials, $V \propto \phi^{-\alpha}$ [2, 3, 4, 5]. If a model is of the former type then its equation of state must be similar to the equation of state of the other components of the cosmic fluid w_f and, indeed, it is even possible during some epochs for the two to be equal. The Quintessence models we are considering are exactly of this type.

Any potential that fulfills the relationship $w_Q = w_f$ must reduce to the exponential potential [76] [5] $V \propto \exp(-\lambda\phi)$ though the Inverse Power Law potential fulfills this requirement when $\alpha \rightarrow \infty$ as may other potentials in appropriate limits. This popular potential has been investigated by Ferreira & Joyce [6], Liddle & Scherrer [5] and Copeland, Liddle & Wands [7], amongst others who showed that the density parameter of the tracker solution for the field [77] is given by $\Omega_Q = 3(w_f + 1)/\lambda^2$.

Note the value of Ω_Q is larger during radiation domination than during matter domination: $\Omega_Q^{(RD)} > \Omega_Q^{(MD)}$. The increase in energy density results in a swifter expansion and the age of the Universe at a fixed scale factor, again given by equation (2), is smaller than that of the standard model by the approximate factor $1/\sqrt{1-\Omega_Q}$. However, by itself, the exponential potential is incapable of leading to an accelerating Universe dominated by dark energy if the Quintessence field has reached it's tracker solution. In order to account for this observation the potential must depart from this simple form as the field and the Universe evolve. More precisely, the field must become dominated by its potential energy in order for $w_Q < -1/3$. There are many ways to achieve this result by modifying the potential from its pure exponential form. One modification, which we will not discuss here, was proposed in Dodelson, Kaplinghat & Stewart [9]. Instead, for our analysis we have selected the Albrecht-Skordis (AS) model [8] where the potential is of the form of a product of a polynomial (quadratic in this case) in ϕ and the exponential,

$$V(\phi) = [(\phi - \phi_0)^2 + A] \exp(-\lambda \phi). \quad (5)$$

The polynomial introduces a local minimum and maximum into the potential and the parameter A must satisfy $A \leq 1/\lambda^2$ in order for the minimum to be at a real value of ϕ [10]: for specificity we have chosen $A\lambda^2 = 1/100$. With this choice for $A\lambda^2$ the two extrema are then very close to ϕ_0 and $\phi_0 + 2/\lambda$. The tracker solution for ϕ thus evolves according to the pure exponential potential at early times when $\phi \ll \phi_0$. As ϕ evolves and approaches the minimum at ϕ_0 the polynomial steepens the potential relative to the exponential resulting in an increase of $\dot{\phi}$ and a simultaneous decline in the potential energy. This phase of $w_Q > w_f$ leads to a significant decrease in Ω_Q . The field passes through ϕ_0 whereupon w_Q begins to decrease as the field climbs out of the minimum. When $w_Q = w_f$ again Ω_Q reaches its minimum value. If the local maximum of the potential is sufficiently high the field is unable to pass over the maximum at $\phi_0 + 2/\lambda$ and resume the exponential scaling behavior, instead it becomes trapped and begins oscillating around ϕ_0 with an ever decreasing amplitude. After several oscillations the kinetic energy has decreased sufficiently and $w_Q \sim -1$ at which point the field begins to mimic a cosmological constant.

On a technical note, while it may appear that we have two remaining free parameters in $V(\phi)$ after specifying $A\lambda^2$, the solution of equation (4) depends upon H which in turn is a function of Ω_{M0} and H_0 . If we fix the geometry of the Universe to be flat then we have specified the energy density of the field at the present time and so introduced a constraint and eliminated another degree of freedom. This leaves only one remaining free parameter which we choose to be λ . Then, assuming the amplitude of the oscillations around the minimum are negligible at the present time, the imposition of the boundary condi-

tions leads to the result that $\lambda\phi_0 \propto -2 \ln \lambda$. Also, from our numerical calculations, we find that the minimum value of Ω_Q is proportional to λ^2 which implies that the redshift at which the field begins to resemble a cosmological constant, z_Λ , increases with λ . We find that roughly $z_\Lambda \approx 4.7 \lambda^{2/3}$ or equivalently $z_\Lambda \approx 7.5 (\Omega_Q^{(RD)})^{-1/3}$.

“G”

A third example of “new physics” is the more radical proposal of a non-minimal coupling between the Ricci scalar, R , and a scalar field which we will further promote to the role of a Quintessence dark energy. This extension therefore requires the postulation of the form of the coupling in addition to the potential $V(\phi)$. Again there are many different models in the literature from which to choose each involving a different form for the coupling and the potential. A very interesting general feature of this class of models is that the strength of the effective gravitational constant during the early evolution of the universe may differ from its current value, which is fixed by terrestrial and solar system experiments. For this reason, we label these models by “G”. While it is possible to derive a general formalism for the cosmology and the evolution of perturbations [11, 12, 13] there is no universal behavior and therefore it becomes necessary to restrict ourselves to a specific example. The model we have adopted here is the minimal extension of the Non-Minimally Coupled (NMC) model investigated by Chen, Scherrer & Steigman [14] and Baccigalupi, Matarrese & Perrotta [15] amongst others. In this model the action takes the form

$$S = \int d^4x \sqrt{-g} \left[\frac{F(\phi) R}{2} - \frac{\phi^{;\mu} \phi_{;\mu}}{2} - V(\phi) + \mathcal{L}_f \right] \quad (6)$$

with $F(\phi) = 1 + \xi(\phi^2 - \phi_0^2)$, ϕ_0 is the value of the field today, and ξ is the coupling constant. From the action we can define the cosmological gravitational parameter to be $1/F$ and so the evolution of the field, and therefore F , will lead to an evolution of the strength of gravity. The potential is taken to be the previously mentioned Inverse Power Law $V = V_0 \phi^{-\alpha}$ which is known to be a viable Quintessence model in the minimally coupled limit [5]. There are two distinct approaches to modifications that arise in these scenarios: redefine the energy density and pressure of the field leaving the cosmological equations unaltered or, adopt the minimally coupled definitions and work with the modified cosmological equations. Both approaches are, of course, equivalent and here we adopt the latter. As a result, the Friedmann equation is modified, becoming

$$H^2 + \frac{H \dot{F}}{F} = \frac{\rho}{3F} \quad (7)$$

and, after introducing the function E , defined by

$$E \equiv 1 + \frac{3F\dot{\phi}^2}{2F}, \quad (8)$$

the field evolves according to the equation

$$\begin{aligned} \ddot{\phi} + 3H\dot{\phi} + V_\phi &= \frac{F_\phi R}{2} \\ &= \frac{F_\phi}{2FE} \left(\rho - 3P + 3F_\phi V_\phi - 3F_{\phi\phi} \dot{\phi}^2 \right). \end{aligned} \quad (9)$$

The presence of the right hand side of equation (9) has been dubbed the R-boost [15]. Examining the right hand side of equation (9) we discover that the last two terms in parentheses on the right-hand side of the equation combine to give a contribution of

$$F_\phi V_\phi - F_{\phi\phi} \dot{\phi}^2 = -\xi(1+\alpha)\rho_G - \xi(1-\alpha)P_G \quad (10)$$

for this potential and coupling. Again we must enforce a self-consistent cosmology because the Hubble parameter is still a function of Ω_{M0} and H_0 so we must adjust the normalization constant in the potential, V_0 , to ensure the boundary conditions are matched.

The Inverse Power Law potential in the minimally coupled limit ($\xi \rightarrow 0$) is a well known and frequently studied Quintessence model [5]. The energy density of the field is negligibly small during the early Universe so that H is dominated by the radiation and matter densities until close to the present time. The tracker solution for ϕ is $\phi \propto a^{3(w_f+1)/(\alpha+2)}$ and for $\alpha = \mathcal{O}(1)$ we can immediately see that, for the tracker solution, $\phi \ll \phi_0$ during much of the evolution of the Universe. The equation of state for the field is

$$w_G = \frac{\alpha w_f - 2}{\alpha + 2} \quad (11)$$

which is always smaller than w_f and so the Quintessence energy density grows relative to the matter + radiation fluid [78]. This solution is also stable in the sense that perturbations from the tracker behavior are damped [5]. The energy density of the field scales as $\rho_G \propto a^{-3\alpha(w_f+1)/(\alpha+2)}$. As we approach the present era the equation of state for the field begins to deviate from the analytic formula in equation (11) and begins to approach $w_G = -1$. The emergence of ρ_G , together with the descending w_G , launches a phase of cosmological acceleration. As α increases the redshift at which the departure from equation (11) occurs also increases but the redshift at which the Universe begins to accelerate falls because while the Quintessence equation of state is no longer given by equation (11) its present value is still correlated with α with smaller α leading to values of w_G that are closer to -1 [19]. For the concordance model parameters $\Omega_{M0} = 0.3$, $\Omega_{G0} = 1 - \Omega_{M0} = 0.7$, $H_0 = 72 \text{ kms}^{-1}\text{Mpc}^{-1}$, the equation of state at the present time is larger than $-1/3$ for $\alpha \gtrsim 8$ while the requirement that the Universe be accelerating requires $\alpha \lesssim 4$ [19].

As with our minimally coupled case “Q” we shall assume that the field has reached its tracker solution long before BBN and so our initial condition for ϕ is this limit during the radiation dominated epoch. This may seem

a minor point but the evolution of the field in its non-tracker state will be very different from its behavior in the tracker solution. We posit that the tracker solutions for non-zero ξ are the same as in the minimally coupled limit and so we must show that the R-boost is negligibly small at early times (*i.e.*, it diverges with a at a slower rate than V_ϕ as $a \rightarrow 0$). The coupling F is almost constant and $F_\phi \propto \phi$ is very small so the scaling of the R-boost during this phase is controlled by whether $\rho_M \propto a^{-3}$ or $\rho_G \propto a^{-4\alpha/(\alpha+2)}$ is the more divergent: for $\alpha < 6$ it is ρ_M otherwise it is ρ_G . So we see that the two terms in equation (9) scale as $V_\phi \propto a^{-4(\alpha+1)/(\alpha+2)}$ while $F_\phi R \propto a^{-(2+3\alpha)/(\alpha+2)}$ for $\alpha < 6$, $F_\phi R \propto a^{(4-4\alpha)/(\alpha+2)}$ for $\alpha > 6$. Thus the derivative of the potential diverges more rapidly than the R-boost whatever the value of α and the tracker solution during radiation domination is identical to the solution in the minimally coupled limit. It could be argued that $\rho_M \rightarrow 0$ as $a \rightarrow 0$ because there are no non-relativistic particles at such high temperatures in which case $R \propto a^{-4\alpha/(\alpha+2)}$ independent of α but this makes no difference to our conclusion. This tracker solution is also stable for any value of ξ as shown by Baccigalupi, Matarrese and Perrotta [15] who relied on the fact that F is virtually constant in order to generalize the result of Uzan [18]. During matter domination the situation is slightly different: $\phi \propto a^{3/(\alpha+2)}$ so both V_ϕ and $F_\phi R$ scale as $a^{-3(\alpha+1)/(\alpha+2)}$ and, therefore, the tracker solution is again the minimally coupled tracker but the normalization changes to account for the presence of the R-boost.

Since $F_\phi R$ scales more slowly than the derivative of the potential during the radiation dominated epoch it might be expected that eventually an R-boost phase will occur: we can estimate the scale factor at which the two are equal to be $a \sim a_{eq}/\xi$ where a_{eq} is the scale factor at radiation-matter equality. An R-boost phase will only occur if $\xi \gtrsim 1$ and, once initiated, will continue into matter domination. If ξ is small then no R-boost phase will occur during radiation domination and neither will it commence during the matter dominated epoch. R-boost phases can occur when the initial value of ϕ differs from the tracker value. In this case, if we again assume F is almost constant and again approximate R as $R = \rho_M/F$, the solution for ϕ during the radiation dominated epoch is

$$\phi = \frac{\phi_\star}{\beta} \sqrt{\frac{a_\star}{a}} J_1 \left(2\beta \sqrt{\frac{a}{a_\star}} \right) \quad \text{for } \xi < 0, \quad (12)$$

$$\phi = \frac{\phi_\star}{\beta} \sqrt{\frac{a_\star}{a}} I_1 \left(2\beta \sqrt{\frac{a}{a_\star}} \right) \quad \text{for } \xi > 0 \quad (13)$$

where $\beta^2 = 3|\xi|\Omega_{M\star}$ and ϕ_\star is the value of the field at a_\star , J_1 and I_1 are the Bessel and modified Bessel functions of the first with index 1. In either case, when the argument of the Bessel function is small ϕ evolves as

$$\phi \approx \phi_\star \left\{ 1 \mp \frac{\beta^2}{2} \left(\frac{a}{a_\star} \right) + \dots \right\}, \quad (14)$$

the minus (plus) sign is for $\xi < 0$ ($\xi > 0$). Note that when $\xi < 0$ the field moves backwards. The very slow change of ϕ justifies the assumption that F is almost constant but, in contrast with the tracker solution, here the behavior arises because ϕ is essentially fixed rather $\phi \ll \phi_0$. During this R-boost phase $\dot{\phi} \propto 1/a$ and the potential energy is much smaller than the kinetic energy so that $w_G \rightarrow 1$ but $\rho_G \propto 1/a^2$, very different from the minimally coupled limit. Eventually any R-boost phase will terminate and the field will follow the tracker solution but, if ϕ_* is much larger than the tracker value, there may be a very long delay before this occurs. The approximate scale factor at which the R-boost phase ends is given by $a = a_*(\phi_*/\phi(a_*))^{(\alpha+2)/4}$.

With the coupling F almost constant during the early Universe and the Quintessence energy density entirely negligible equation (7) essentially reduces to the Friedmann equation of our standard model except for an effective gravitational strength $G' = G/F$. Therefore the only change is to the age of the Universe at a given scale factor, once again given by equation (2), which is simply rescaled by the factor \sqrt{F} . If F were not constant, and could be adequately described by a power law function of the scale factor, then we would attain the circumstances investigated by Carroll and Kaplinghat [17].

The evolution of the field becomes more complicated as the present epoch is approached: the R-boost is no longer negligible, F starts to change noticeably and the field's energy density becomes important. Again the equation of state for the field begins to descend towards $w_G = -1$ but the exact evolution is now also a function of ξ . This can be understood from the evolution of ρ_G which is

$$\dot{\rho}_G + 3H(\rho_G + P_G) = \frac{\dot{F}R}{2}. \quad (15)$$

The power source $\dot{F}R/2$ is proportional to ξ so if $\xi > 0$ then the field gains energy relative to a field in the minimally coupled limit if $R > 0$. The power source will become a drain if or when R switches sign as the Universe begins to accelerate. The increase in energy density results in an increase in the equation of state relative to the minimal case and thus a relative increase in $\dot{\phi}$ and ϕ . The increased energy density will terminate matter domination at a higher redshift.

Finally we impose the constraints on the model parameters from the timing experiment using the Viking probe and from limits to the evolution of the strength of gravity [16]. The first constraint, the more severe of the two, is

$$\xi \phi_0 < 0.022 \quad (16)$$

while the second limits

$$2\xi \phi_0 \dot{\phi}_0 < 10^{-11} \text{ yr}^{-1} \quad (17)$$

where $\dot{\phi}_0$ is time derivative of the field at the present epoch. As shown in Chen, Scherrer and Steigman [14], ϕ_0 is very weakly dependent upon ξ so that it is essentially

determined by α and V_0 . Therefore, with fixed values of α and V_0 , the limit in equation (16) is essentially a limit on ξ or, if F_{BBN} is the (almost constant) value of F during BBN and if ϕ during this epoch is much smaller than ϕ_0 , then

$$\xi = \frac{1 - F_{BBN}}{\phi_0^2} \quad (18)$$

and the limit on ξ therefore becomes a limit on F_{BBN} or, equivalently, on G'/G . From our numerical calculations, again with the concordance model parameters, we find that G'/G is restricted to lie between

$$\begin{aligned} 0.976 &\leq G'/G \leq 1.025 & \alpha &= 1, \\ 0.964 &\leq G'/G \leq 1.040 & \alpha &= 2, \\ 0.942 &\leq G'/G \leq 1.067 & \alpha &= 4. \end{aligned} \quad (19)$$

III. BIG BANG NUCLEOSYNTHESIS

To better appreciate the similarities and differences among the three candidates for “new” physics under consideration here (equivalent neutrinos: “X”; Quintessence: “Q”; non-minimal coupling: “G”) it will be helpful to briefly review “standard” BBN (SBBN). To this end the discussion may begin when the universe is a few tenths of a second old and the temperature is a few MeV. The energy density receives its dominant contributions from the relativistic particles present; prior to e^\pm annihilation these are: CBR photons, e^\pm pairs, and three flavors of neutrinos,

$$\rho_R = \rho_\gamma + \rho_e + 3\rho_\nu = \frac{43}{8}\rho_\gamma. \quad (20)$$

At this time ($T \sim$ few MeV) the neutrinos are beginning to decouple from the photon - e^\pm plasma and the neutron to proton ratio, crucial for the primordial abundance of ${}^4\text{He}$, is decreasing. As the temperature drops below ~ 2 MeV, the two-body collisions interconverting neutrons and protons become too slow to maintain equilibrium and the neutron-to-proton ratio begins to deviate from (exceeds) its equilibrium value ($(n/p)_{eq} = \exp(-\Delta m/T)$). Prior to e^\pm annihilation, at $T \approx 0.8$ MeV when the universe is ≈ 1 second old, the two-body reactions regulating the n/p ratio become too slow compared to the universal expansion rate and this ratio “freezes in”, although it actually continues to decrease due to the emerging importance of ordinary beta decay ($\tau_n = 885.7$ sec.). Since there are several billion CBR photons for every nucleon (baryon), no complex nuclei exist at these early times.

BBN begins in earnest after e^\pm annihilation, at $T \approx 0.08$ MeV ($t \approx 3$ minutes), when the number density of CMB photons with enough energy to photodissociate deuterium (those in the tail of the black body distribution) is comparable to the baryon density. By this time the n/p ratio has further decreased due to beta decay, limiting (mainly) the amount of helium-4 which can be

synthesized. As a result, the predictions of primordial nucleosynthesis depend sensitively on the early expansion rate. In SBBN it is assumed that the neutrinos are fully decoupled prior to e^\pm annihilation and don't share in the energy transferred from the annihilating e^\pm pairs to the CMB photons. Thus, in the post- e^\pm annihilation universe the photons are hotter than the neutrinos and,

$$\rho_R = \rho_\gamma + 3\rho_\nu = 1.6813\rho_\gamma. \quad (21)$$

During these RD epochs the age and the energy density are related by $\frac{4}{3}\rho_R t^2 = 1$ (recall that we have chosen units in which $8\pi G = 1$), so that the age of the universe is known (as a function of the CMB temperature) once the particle content (ρ_R) is specified **and** the strength of the gravitational interaction (G) is fixed. In the standard model,

$$\text{Pre} - e^\pm \text{ annihilation : } t T_\gamma^2 = 0.738 \text{ MeV}^2 \text{ s}, \quad (22)$$

$$\text{Post} - e^\pm \text{ annihilation : } t T_\gamma^2 = 1.32 \text{ MeV}^2 \text{ s}. \quad (23)$$

The BBN-predicted abundances of deuterium, helium-3 and lithium are determined by the competition between various two-body production/destruction rates and the universal expansion rate, while the helium-4 abundance depends most directly on the neutron abundance at the time BBN begins. As a result, the D, ^3He , and Li abundances are sensitive to the post- e^\pm annihilation expansion rate, while that of ^4He depends on **both** the pre- and post- e^\pm annihilation expansion rates; the former determines the “freeze-in” and the latter the importance of beta decay. Of course, the BBN abundances do depend on the baryon density ($\eta_{10} \equiv 10^{10} n_B/n_\gamma = 274\Omega_B h^2$), so that the abundances of at least two different relic nuclei are needed to break the degeneracy between the baryon density and a possible non-standard expansion rate resulting from new physics or cosmology.

A. Non-Standard BBN

Our simplest alternative to the standard cosmology is the scenario of extra relativistic energy denoted by “ X ”. When X is decoupled in the sense that it doesn't share in the energy released in e^\pm annihilation, it is convenient to account for this extra contribution to the standard-model energy density by normalizing it to that of an extra, “equivalent” neutrino flavor [20],

$$\rho_X \equiv \Delta N_\nu \rho_\nu = \frac{7}{8} \Delta N_\nu \rho_\gamma. \quad (24)$$

For each such “neutrino-like” particle (*i.e.*, a two-component fermion), if $T_X = T_\nu$, then $\Delta N_\nu = 1$; if X is a scalar, $\Delta N_\nu = 4/7$. However, it may well be that X has decoupled earlier in the evolution of the universe and has failed to profit from the heating when various other

particle-antiparticle pairs annihilated (or unstable particles decayed). In this case, the contribution to ΔN_ν from each such particle will be < 1 ($< 4/7$). Since we are interested in different models of non-standard physics resulting in modifications to the standard model energy density and expansion rate, henceforth this case will be identified by a superscript, X ; $\Delta N_\nu = \Delta N_\nu^X$.

In the presence of this extra component, the pre- e^\pm annihilation energy density in equation (20) is modified to,

$$(\rho_R)_{pre}^X = \frac{43}{8} \left(1 + \frac{7\Delta N_\nu^X}{43} \right) \rho_\gamma. \quad (25)$$

The extra energy density speeds up the expansion of the universe so that the right hand side of the time-temperature relation in equation (22) is smaller by the square root of the factor in parentheses in equation (25).

$$\begin{aligned} S_{pre}^X \equiv (t/t')_{pre} &= \left(1 + \frac{7\Delta N_\nu^X}{43} \right)^{1/2} \\ &= (1 + 0.1628\Delta N_\nu^X)^{1/2}. \end{aligned} \quad (26)$$

In the post- e^\pm annihilation universe the extra energy density contributed by the X s is diluted by the heating of the photons, so that,

$$(\rho_R)_{post}^X = 1.6813(1 + 0.1351\Delta N_\nu^X)\rho_\gamma, \quad (27)$$

and

$$S_{post}^X \equiv (t/t')_{post} = (1 + 0.1351\Delta N_\nu^X)^{1/2}. \quad (28)$$

These relations (eqs. 25-28) may now be generalized to the two other cases under consideration.

For our minimally coupled Quintessence model “ Q ” the energy density of the field during radiation domination (relevant to BBN), is $\Omega_Q^{(RD)} = 4/\lambda^2$. This extra energy density may be written in terms of an equivalent ΔN_ν^Q ,

$$\Delta N_\nu^Q \equiv \frac{43}{7} \left(\frac{\Omega_Q^{(RD)}}{1 - \Omega_Q^{(RD)}} \right). \quad (29)$$

Since, for this Quintessence model, the scalar field contributes the *same fraction* of the total (radiation) energy density pre- and post- e^\pm annihilation,

$$(\rho_R)_{pre}^Q = (\rho_R)_{post}^Q = \frac{43}{8} \left(1 + \frac{7\Delta N_\nu^Q}{43} \right) \rho_\gamma, \quad (30)$$

and

$$S_{pre}^Q = S_{post}^Q \equiv S^Q = (1 + 0.1628\Delta N_\nu^Q)^{1/2}, \quad (31)$$

Thus for this class of Quintessence models the speed-up factor (S^Q) in the universal expansion rate prior to e^\pm annihilation is the *same* as the speed-up factor

after e^\pm annihilation. In comparing with the equivalent neutrino case, we see that for $\Delta N_\nu = \Delta N_\nu^X = \Delta N_\nu^Q$, the post- e^\pm annihilation universe expands faster for “Q” than for “X”; alternately, for the *same* post- e^\pm annihilation speed-up, $\Delta N_\nu^Q \approx 0.83\Delta N_\nu^X$.

In our non-minimally coupled Quintessence model, “G”, the Quintessence energy density during BBN is entirely negligible hence the total energy density at a given redshift is unaltered,

$$(\rho_R)^G = \rho_R \quad (32)$$

where ρ_R is given by eqs. 25 and 27 for the pre- and post- e^\pm annihilation universe respectively. However, since $t \propto (G\rho_R)^{-1/2}$,

$$S_{pre}^G = S_{post}^G = (G'/G)^{1/2} \equiv \left(1 + \frac{7\Delta N_\nu^G}{43}\right)^{1/2}. \quad (33)$$

For this case we have defined an equivalent number of extra neutrinos by

$$\Delta N_\nu^G \equiv \frac{43}{7} \left(\frac{\Delta G}{G}\right). \quad (34)$$

As with Quintessence, the non-minimally coupled scalar fields result in faster expansion of the post- e^\pm annihilation universe for the *same* increase in the pre- e^\pm annihilation expansion rate. Thus, for the same ΔN_ν the effects on BBN of “Q” and “G” are identical, but they do have the potential to be different from those due to the usual example of extra energy density in the form of equivalent neutrinos (“X”). However there is one important difference between “Q” and “G”, namely that ΔN_ν^Q is unconstrained (at the moment) while the limits expressed in (16) and (17) translate to a restricted range for ΔN_ν^G . The range for ΔN_ν^G is a function of α , the exponent of the Inverse Power Law potential and, as shown in Chen, Scherrer and Steigman [14], the limits increase with the exponent.

On the basis of the above discussion the results of our detailed BBN calculations may be understood. Since the primordial abundances of D, ^3He , and Li freeze-in late, well after e^\pm annihilation has occurred, they mainly provide a probe of S_{post} . In contrast, the ^4He mass fraction, Y_P , retains sensitivity to *both* S_{pre} and S_{post} . Furthermore, while the abundances of D, ^3He , and Li are most sensitive to the baryon density, the ^4He mass fraction provides the best probe of the expansion rate. This is illustrated in Figure 1 where, in the $\Delta N_\nu - \eta_{10}$ plane are shown isoabundance contours for D/H and Y_P (the isoabundance curves for $^3\text{He}/\text{H}$ and for Li/H , omitted for clarity, are similar in behavior to that of D/H). While the solid curves are for the “usual” extra energy density in relativistic particles, the dashed curves show, for the same equivalent ΔN_ν (see eqs. 29 & 34), the modifications to SBBN for both minimally and non-minimally coupled scalar fields. The trends illustrated in Figure 1 are easy to understand in the context of our discussion

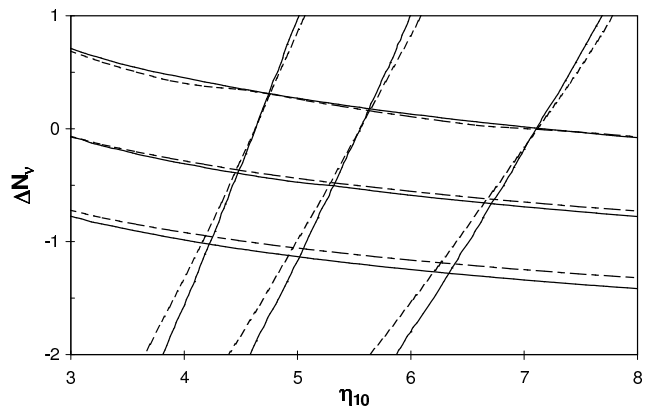


FIG. 1: Isoabundance curves for D and ^4He in the $\Delta N_\nu - \eta_{10}$ plane. The solid curves are for $\Delta N_\nu = \Delta N_\nu^X$, while the dashed curves correspond to the minimally and non-minimally coupled scalar field cases where $\Delta N_\nu = \Delta N_\nu^G = \Delta N_\nu^Q$. For ^4He the curves (nearly horizontal) are for, from top to bottom: $Y = 0.25, 0.24, 0.23$. For D the curves (nearly vertical) are for, from left to right: $10^5(\text{D}/\text{H}) = 4.0, 3.0, 2.0$.

above of SBBN. The higher the baryon density (η_{10}), the faster primordial D is destroyed, so D/H is anticorrelated with η_{10} . But, the faster the universe expands ($\Delta N_\nu > 0$), the less time is available for D-destruction, so D/H is positively correlated with ΔN_ν . Since for the *same* ΔN_ν , the post- e^\pm annihilation universe expands more rapidly for “ ϕ ” and “G” than for “X”, the D-isoabundance curves differ slightly as shown in Figure 1. In contrast to D (and to ^3He and Li), the ^4He mass fraction is relatively insensitive to the baryon density, but is very sensitive to both the pre- and post- e^\pm annihilation expansion rates (which control the neutron-to-proton ratio). The faster the universe expands, the more neutrons are available for ^4He . Again, the effect on Y_P of the same ΔN_ν is slightly different for “X”, than for “Q” and “G”, as seen in Figure 1.

B. Primordial Abundances

It is clear from Figure 1 that any BBN constraints on new physics will be data-driven. While D (and/or ^3He and/or Li) largely constrain the baryon density and ^4He plays the same role for ΔN_ν , there is an interplay between η_{10} and ΔN_ν which is quite sensitive to the adopted abundances. For example, a lower primordial D/H increases the BBN-inferred value of η_{10} , leading to a higher predicted primordial ^4He mass fraction. If the primordial ^4He mass fraction derived from the data is “low”, then a low upper bound on ΔN_ν will be inferred. It is, therefore, crucial that we make every effort to avoid biasing our conclusions by underestimating the uncertainties at present in the primordial abundances de-

rived from the observational data. To this end, first of all we concentrate on deuterium as the baryometer of choice since its observed abundance should have only decreased since BBN [21] and the deuterium observed in the high redshift, low metallicity QSO absorption line systems (QSOALS) should be very nearly primordial. The post-BBN evolution of ${}^3\text{He}$ and of Li are likely more complicated, involving competition between production, destruction, and survival.

Even so, inferring the primordial D abundance from the QSOALS has not been without its difficulties, with some abundance claims withdrawn or revised. At present there are 4 – 5 QSOALS with reasonably firm deuterium detections [22, 23, 24, 25, 26]. However, when D/H is plotted as a function of metallicity or redshift, there is significant dispersion and the data fail to reveal the anticipated “deuterium plateau” [27]. Furthermore, subsequent observations of the D’Odorico *et al.* [26] QSOALS by Levshakov *et al.* [28] revealed a more complex velocity structure and led to a revised – and uncertain – deuterium abundance. This sensitivity to the often poorly constrained velocity structure in the absorbers is also exposed by the analyses of published QSOALS data by Levshakov and collaborators [29, 30, 31], which lead to consistent but somewhat higher deuterium abundances than those inferred from “standard” data reduction analyses. Given this current state of affairs we believe that while the O’Meara *et al.* [24] estimate for the primordial abundance is likely accurate ($\text{D}/\text{H} = 3.0 \times 10^{-5}$), their error estimate ($\pm 0.4 \times 10^{-5}$) may be too small. At the risk of erring on the side of caution, here we adopt a range which encompasses the uncertainties referred to above: $\text{D}/\text{H} = 3.0_{-0.5}^{+1.0} \times 10^{-5}$. Although permitting a larger than usual range in baryon density, this choice has little direct effect on the probe of new physics (constraints on ΔN_ν) which is the focus of this study.

A similarly clouded situation exists for the primordial abundance of ${}^4\text{He}$. At present there are two estimates for the primordial abundance of ${}^4\text{He}$ based on large, nearly independent data sets and analyses of low-metallicity, extragalactic H II regions. The “IT” [32, 33] estimate of $Y_{\text{P}}(\text{IT}) = 0.244 \pm 0.002$ and the “OS” determination [34, 35, 36] of $Y_{\text{P}}(\text{OS}) = 0.234 \pm 0.003$ which is nearly 3σ lower. Recent high quality observations of a relatively metal-rich H II region in the Small Magellanic Cloud (SMC) by Peimbert, Peimbert, and Ruiz (PPR) [37] reveal an abundance $Y_{\text{SMC}} = 0.2405 \pm 0.0018$. When this abundance is extrapolated to zero metallicity, PPR find $Y_{\text{P}}(\text{PPR}) = 0.2345 \pm 0.0026$, lending some support to the lower OS value. These comparisons among different observations suggest that unaccounted systematic errors may dominate the statistical uncertainties. Indeed, Gruenwald, Steigman, and Viegas [38] argue that if unseen neutral hydrogen in the ionized helium region of the observed H II regions is accounted for, the IT estimate of the primordial abundance should be reduced to $Y_{\text{P}}(\text{GSV}) = 0.238 \pm 0.003$ (see also [39, 40]). Here, we adopt this latter estimate for the central value

but, as we did with deuterium, the uncertainty is increased in an attempt to account for likely systematic errors: $Y_{\text{P}} = 0.238 \pm 0.005$, leading to a 95% CL range, $0.228 \leq Y_{\text{P}} \leq 0.248$; this is in agreement with the estimate adopted by Olive, Steigman, and Walker [41] in their review of SBBN.

C. Constraints From BBN

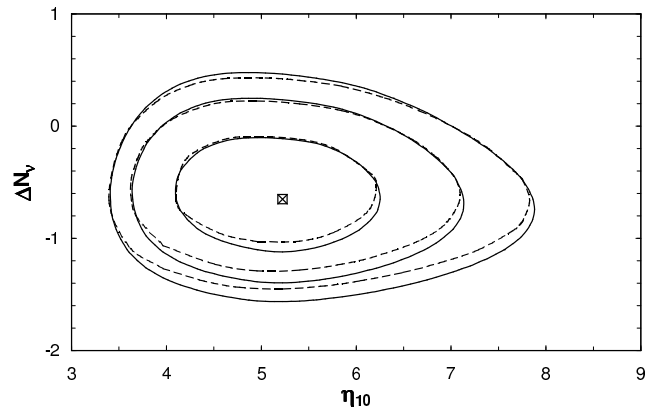


FIG. 2: Likelihood contours (68%, 95% and 99% respectively) in the $\Delta N_\nu - \eta_{10}$ plane. The solid curves are for $\Delta N_\nu = \Delta N_\nu^X$, while the dashed curves correspond to the minimally and non-minimally coupled scalar field cases where $\Delta N_\nu = \Delta N_\nu^G = \Delta N_\nu^Q$. The best fit points are indicated by the cross for “X”, and the square for “Q”/“G”.

Using the abundance ranges adopted above, we have calculated the $\Delta N_\nu - \eta_{10}$ likelihood contours which are shown in Figures 2 & 3. A simple, semi-quantitative analysis can serve to shed light on the detailed results shown in Figures 2 & 3. As revealed in Figure 1, the baryon density is primarily fixed by deuterium. For $\text{D}/\text{H} = 3.0 \times 10^{-5}$, $\eta_{10} \approx 5.6$ ($\Omega_{\text{B}} \approx 0.020$). In contrast, ΔN_ν is most sensitive to ${}^4\text{He}$; $\Delta Y \approx 0.013 \Delta N_\nu$. For $\eta_{10} \approx 5.6$ and $\Delta N_\nu = 0$, $Y_{\text{P}} = 0.247$. Comparing this with the central value (0.238) or the 2σ upper bound (0.248) inferred from the data, it can be expected that $\Delta N_\nu \approx -0.7$ and $\Delta N_\nu \lesssim +0.1$ respectively. In fact, the detailed calculations reveal that the “best” value for “X” is $\Delta N_\nu = -0.65$, while for “G/Q”, $\Delta N_\nu = -0.58$; the 2σ upper bounds are $\Delta N_\nu \leq +0.04$ in all three cases, corresponding to the bound $\Omega_Q^{(RD)} \leq 0.007$ for the Quintessence model ($\lambda \geq 25$). If in place of our adopted central value and range for Y_{P} , those from IT had been chosen, the contours in Figures 2 & 3 would shift upwards by $\Delta N_\nu \approx 0.5$ and they would be narrower in the vertical direction. However, since at 95% CL the two estimates for Y_{P} agree, the upper bounds to ΔN_ν will be closely equal. While we are most concerned with the BBN constraints

on ΔN_ν , we note in passing that the best estimate for the baryon density is $\eta_{10} \approx 5.2$ ($\Omega_B h^2 \approx 0.019$).

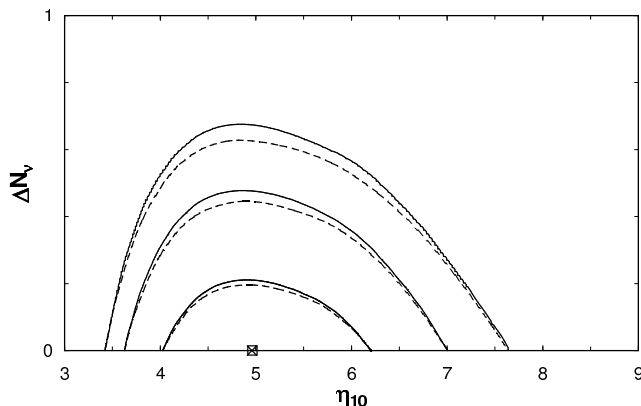


FIG. 3: Likelihood contours as in Figure 2, but with the restriction that $\Delta N_\nu \geq 0$. The best fit points are indicated by the cross for “X”, and the square for “Q”/“G”.

We must point out that there is a logical inconsistency in the above analysis. Firstly, for two of the cases we (and others before us) have been considering, “X” and “Q”, the energy density and expansion rate during BBN are only *increased* compared to those for SBBN [79]. Since it is well established that there are three, very light (hence, relativistic at BBN) neutrinos, $N_\nu \geq 3$ and $\Delta N_\nu \geq 0$. Only our “G” case can naturally accommodate $S < 1$ and, hence, $\Delta N_\nu < 0$ (see, *e.g.*, Chen, Scherrer, and Steigman [14]). In Figure 3 are displayed the corresponding likelihood contours when the restriction $\Delta N_\nu \geq 0$ is imposed. The “best fit” now occurs for $\Delta N_\nu = 0$ and $\eta_{10} = 5.0$ ($\Omega_B h^2 = 0.019$). In this case the upper bounds on ΔN_ν are increased relative to those when ΔN_ν is left free to be negative as well as positive; at 95% CL, $\Delta N_\nu \leq 0.43$ for “X” and $\Delta N_\nu \leq 0.39$ for “Q”. For the Quintessence model this corresponds to the bound $\Omega_Q^{(RD)} \leq 0.060$ ($\lambda \geq 8.2$). From a similar analysis ($\Delta N_\nu \geq 0$), but using the narrower range of the IT ${}^4\text{He}$ abundance as well as the O’Meara *et al.* [24] narrow deuterium range, Bean, Hansen, and Melchiorri [44] find a 95% upper bound of $\Omega_Q \leq 0.045$ ($\lambda \geq 9.4$).

Secondly, as mentioned before in §II, the range of ΔN_ν^G is constrained by the experimental limits on the present-day deviation from GR as indicated by the allowed ranges of G listed in (19). The permitted ranges of ΔN_ν^G are, therefore, a function of α . Without (yet) imposing a restriction on this parameter, the range in ΔN_ν is otherwise unconstrained.

As the results here demonstrate, BBN can impose significant constraints on these non-standard models, noticeably restricting the choice of the additional parameters which accompany the new physics. The changes in the dynamics and evolution of the universe imposed by these models continues after BBN, up to the present

epoch. We turn next to the effects on the formation of the CMB anisotropy spectrum and the constraints which may be imposed on these models by the current observational data.

IV. STANDARD CMB

In order to understand the effects of new physics upon the formation of the anisotropies in the CMB we briefly review the formation of temperature fluctuations in the standard model. More extensive reviews may be found in Ma and Bertschinger [45], Hu and Sugiyama [46] and elsewhere so we will only outline the general procedure and important results. Hereafter overdots denote derivatives with respect to conformal time τ where $a(\tau) d\tau = dt$ and overbars indicate unperturbed quantities. We shall write the conformal Hubble parameter as \mathcal{H} so that $a \mathcal{H} = da/d\tau$ and therefore

$$\tau(a) = \int_0^a \frac{1}{a \mathcal{H}} da. \quad (35)$$

The CMB anisotropies observed today are the redshifted temperature fluctuations that occurred in the baryon-photon fluid prior to recombination. The stress energy for a perfect fluid with energy density ρ and pressure P is simply $T_\nu^\mu = P g_\nu^\mu + (\rho + P) u^\mu u_\nu$ and the perturbations in the fluid are introduced as $\rho = \bar{\rho} + \delta\rho = \bar{\rho}(1 + \delta)$, $P = \bar{P} + \delta P$ and $u^\mu = \bar{u}^\mu + v^\mu$ but also an anisotropic stress $\Sigma^{\mu\nu} = \bar{P} \Pi^{\mu\nu}$ is included in order to account for shear, viscosity and other such processes [45]. For multiple components the stress energy tensor is the sum of the stress energy tensors of each component i , in our case vacuum (Λ), CDM (C), baryons (B), photons (γ) and neutrinos (ν), so that $\rho = \sum_i \rho_i$, etc. For the relativistic components, such as photons and neutrinos, the treatment as a fluid is unrealistic and, instead, the phase space description must be used. The temperature fluctuation, or brightness function, $\Theta_i = \delta T_i / \bar{T}_i$, is introduced for each relativistic species; the Θ_i are functions of time τ , position \mathbf{x} and the direction cosines $\hat{\mathbf{n}}$ of the particle momenta. There are no fluctuations in the vacuum energy.

The manner in which scalar perturbations in the metric are introduced defines the gauge and many different choices have appeared in the literature. Two of the most popular gauges, the synchronous and the Newtonian, were compared in Ma and Bertschinger [45] and others are discussed by many authors including Hwang [47]. The synchronous gauge is chosen so that the peculiar velocity of the CDM is zero.

The perturbations in all quantities may be decomposed into their Fourier modes (with wavenumber k) and, in addition, the angular dependence in the brightness functions may be expanded as an infinite sum of Legendre polynomials with coefficients Θ_ℓ . In terms of these moments, the thermodynamic equivalents of the energy density,

pressure, and anisotropic stress are

$$\delta\rho_i = 4\Theta_{i0} \quad v_i = \Theta_{i1} \quad \Pi_i = \frac{12}{5}\Theta_{i2} \quad (36)$$

for each relativistic component i .

All that remains is to specify the initial conditions for the perturbations: this is accomplished by examining the behavior on superhorizon scales deep within the radiation dominated epoch, retaining only the growing modes, and relating the perturbations with some ‘principle’ such as adiabatic or isocurvature. For adiabatic initial conditions in the synchronous gauge we have the well known relations [45]:

$$\begin{aligned} \delta_C &= \delta_B = \frac{3}{4}\delta_\gamma = \frac{3}{4}\delta_\nu = C(k\tau)^2 \\ \bar{\rho}_B v_B &= \frac{4}{3}\bar{\rho}_\gamma v_\gamma = \frac{15+4f_\nu}{23+4f_\nu}\bar{\rho}_\nu v_\nu = \frac{k\tau\delta_C}{9} \\ \Pi_\nu &= \frac{-16\delta_C}{3(15+4f_\nu)} \end{aligned} \quad (37)$$

where f_ν is the fraction of the relativistic energy density in neutrinos and C is a dimensionless constant.

The evolution of each mode is a function of its wavelength and of the gauge. All modes begin at superhorizon scale, $k\tau \ll 1$, and the CDM perturbations evolve as $\delta_C \propto k^2\tau^2$ during both matter and radiation domination. As time progresses the horizon becomes bigger than the wavelengths of different modes; modes with larger wavenumbers (smaller wavelengths) enter the horizon before the smaller wavenumber (larger wavelength) modes. The evolution of δ_C for modes that enter the horizon during radiation domination is stunted; they grow only as $\ln\tau$. This stagnation continues until matter domination whereupon the modes begin to grow again as τ^2 . Prior to recombination the behavior of the baryon-photon fluid changes radically as a mode enters the sound horizon $s_{\gamma B}$, which is given by

$$s_{\gamma B}(\tau) = \int_0^\tau d\tau' c_{\gamma B} = \int_0^a \frac{da}{a\mathcal{H}} \sqrt{\frac{\bar{\rho}_\gamma + \bar{P}_\gamma}{\bar{\rho}_\gamma + \bar{P}_\gamma + \bar{\rho}_B}} \quad (38)$$

where $c_{\gamma B}$ is the baryon-photon fluid sound speed. Note the presence of the baryon density in the denominator of equation (38). The perturbations present in the fluid drive oscillations in the baryon density, the peculiar velocity, and the photon brightness function for moments $\ell \in \{0, 1\}$. There are no fluctuations for $\ell > 2$ because of the tight coupling between the photons and baryons and because the isotropising effect of Thompson scattering suppresses these moments. The oscillations are forced by the CDM perturbations via the metric potentials and their amplitude increases with the ratio of the baryon and photon densities. Once initiated, the oscillations continue until recombination at which point the photon-baryon/electron interaction ceases and the photons free-stream. The phase of each mode at recombination is recorded in the anisotropy angular power spectrum

C_ℓ . Recombination, which occurs at τ_* , a_* , introduces an important modification to the C_ℓ known as Silk damping [48] that is due to the increase in photon mean free path as the number of free electrons crashes. The subsequent increase in photon diffusion smoothes temperature fluctuations on scales smaller than this diffusion length. Modification of the Θ_ℓ does not end at recombination: the evolution of the Universe after this time will imprint itself upon brightness function moments through the evolution of the potentials. This change, known as the Integrated Sachs-Wolfe (ISW) effect, is initiated by the fading importance of the radiation density (the early ISW effect) and the growing importance of the vacuum energy towards the present epoch (the late ISW effect). Both cause an increase in the photon temperature variance on the scales at which these processes occur.

What emerges from the detailed calculations is the solution for the evolution of the perturbations, for a given cosmology. The perturbations for each wavenumber are scaled according to an initial power spectrum and normalized, usually to COBE. The photon temperature variance vector C_ℓ , or $\mathcal{C}_\ell = \ell(\ell+1)C_\ell/2\pi$, is then constructed. The spectrum of the C_ℓ consists of a series of peaks at specific ℓ and so the gross features of a model can be characterized by the positions of the peaks, the height of the first peak relative to the COBE normalization point and then the relative heights of all other peaks to the first [49, 50]. Regardless of the curvature of the Universe, the position of the peaks is proportional to the ratio of the comoving angular diameter distance and the size of the sound horizon at last scattering [49]. The height of the first peak is a measure of change in the Universe since last scattering, while the relative heights of the other peaks and the ratios of their separations is set by the astrophysics prior to and during recombination. In general there is a complex interplay between the different elements contributing to the formation of the temperature fluctuation spectrum, but whenever possible we shall try to couch the changes to the CMB in this language.

V. NON-STANDARD CMB

“X”

The inclusion of extra relativistic energy into the CMB calculation is relatively straightforward. As for the photons and the three known neutrino flavors, a brightness function is introduced that is Fourier transformed and the angular dependence expanded in a basis of Legendre polynomials. If we do not allow the extra energy density to interact with the other components (except through gravity) then the set of equations governing the evolution of the brightness function coefficients is exactly the same as for the neutrinos and there is no suppression of the higher moments of the brightness function. The initial conditions for the extra energy density are taken to be

exactly those of the neutrinos so that $N_\nu \rightarrow N_\nu + \Delta N_\nu^X$ and $f_\nu \rightarrow f_\nu + f_X$. The effects of extra relativistic energy density “X” upon the CMB anisotropy power spectrum are then equivalent to an amplification of the neutrino sector. The extra energy will increase the expansion rate \mathcal{H} , with the largest changes, relative to the standard model, occurring during the early, radiation dominated, epoch. The swifter expansion modifies both the time-temperature relationship and leads to an earlier decoupling of the photons since the scattering rate now becomes smaller than \mathcal{H} at an earlier epoch. Therefore both age of the Universe, τ_* , and the scale factor, a_* , at recombination are smaller and from equation (38) we see that this will lead to a smaller sound horizon, $s_{\gamma B}(\tau_*)$. The increase in \mathcal{H} due to the extra energy density will shift in the CMB peaks to smaller angular scales (higher ℓ values) and increase the peak separation. The extra radiation also lowers the redshift of matter-radiation equality which will increase the suppression of the growth of CDM perturbations on subhorizon scales prior to matter domination and cause an increase in the temperature variance [51]. The increase in the Hubble parameter also reduces the contribution to the anisotropy spectrum from the velocity perturbation and the Silk damping is also less effective, further increasing the peak enhancement at large ℓ . Lastly, since the extra energy density associated with “X” can cluster under the influence of gravity, increasing ΔN_ν enhances the early Integrated Sachs-Wolfe (ISW) effect, leading to a significant increase in the height of the first peak relative to the others.

“Q”

In general the perturbations in the Quintessence energy density, pressure, and peculiar velocity, after Fourier transforming to k-space are

$$\delta\rho_Q = \frac{1}{a^2} \bar{\phi} \delta\dot{\phi} + \bar{V}_\phi \delta\phi, \quad (39)$$

$$\delta P_Q = \frac{1}{a^2} \bar{\phi} \delta\dot{\phi} - \bar{V}_\phi \delta\phi, \quad (40)$$

$$v_Q = k \delta\phi / \bar{\phi} \quad (41)$$

and the Klein-Gordon equation for the evolution of the perturbations is simply

$$\delta\ddot{\phi} + 2\mathcal{H}\delta\dot{\phi} + (k^2 + a^2 \bar{V}_{\phi\phi}) \delta\phi - \bar{\phi} \dot{\delta}_C = 0. \quad (42)$$

There is no shear term for the Quintessence field. The density perturbations in the field are not adiabatic [52, 53, 54]. That is, $\delta P_Q - c_Q^2 \delta\rho_Q \neq 0$ where $c_Q^2 = dP_Q/d\rho_Q$ is the adiabatic sound speed, a fact which, according to Ratra & Peebles [54] is “exceedingly fortunate” since pressure fluctuations can resist the collapse of Quintessence density fluctuations even if the equation of state is zero. In principle the CMB anisotropy spectrum emerging from a quintessence model is very different from the case of “X”, but certain effects may be

missing or small depending on the exact behavior of the field.

The changes wrought upon the CMB anisotropy spectrum from replacement of the vacuum energy (Λ) with a Quintessence dark energy that follows the exponential potential were investigated by Ratra & Peebles [54], Ferreira & Joyce [6] and Skordis & Albrecht [52]. Deep in the radiation dominated epoch the AS potential may be approximated by a pure exponential and for this potential, on superhorizon scales and with adiabatic initial conditions, there is no change to the evolution of perturbations, *i.e.*, $\delta_C \propto k^2 \tau^2$ [6], which is wholly expected because during this period the Quintessence equation of state is exactly the same as that of the radiation. The adiabatic initial density fluctuation in Q is simply [6, 52]

$$\delta_Q = \frac{4}{15} \delta_C \quad (43)$$

which translates to a perturbation in the field [52]

$$\delta\phi = 4\delta_C/5\lambda \quad \delta\dot{\phi} = 4\dot{\delta}_C/5\lambda. \quad (44)$$

Though we have used equations (43) and (44) in all our calculations the evolution of the Quintessence perturbations is largely independent of the exact initial conditions of the field when the equation of state is a constant [55].

Life becomes more interesting on subhorizon scales, $k\tau \gg 1$. As in Ferreira & Joyce [6], we take the potential derivative and gravitational feedback terms in equation (42) to be negligible relative to the $k^2\delta_Q$ piece so that, after using $3(\bar{w}_f + 1) - 2 = 2/H\tau$, we obtain

$$\tau^2 \delta\ddot{\phi} + \frac{4\tau}{3(\bar{w}_f + 1) - 2} \delta\dot{\phi} + k^2 \tau^2 \delta\phi \approx 0. \quad (45)$$

The solutions of this equation are linear combinations of $J_p(k\tau)/\tau^p$, $N_p(k\tau)/\tau^p$ with $p = 1/2$ during radiation domination and $p = 3/2$ during matter domination [6]. The subhorizon perturbations in the field oscillate with decaying amplitudes and so Quintessence does not cluster. The density contrast of the CDM continues to grow as $\ln\tau$ during radiation domination, but during matter domination the evolution changes to $\delta_C \propto \tau^{2+\epsilon}$ where

$$2\epsilon = 5\sqrt{1 - 24\Omega_Q^{(MD)}/25} - 5 \leq 0. \quad (46)$$

The lack of clustering in the Quintessence energy density, along with its contribution to \mathcal{H} inhibit growth in the CDM.

These results apply when the Albrecht-Skordis potential may be approximated by a pure exponential but when the polynomial prefactor becomes important, these results break down. However we can anticipate some of the effects of the field from the simple fact that the effect of a significant Quintessence energy density is to drive a swifter expansion. In this regard the “Q” model we have adopted bears some similarity to “X” in that the effect of the extra energy density in the early universe leads to a

smaller sound horizon $s_{\gamma B}(\tau_*)$ at recombination driving the anisotropy spectrum peaks to smaller scales and increasing their separation. At the same time the increase in \mathcal{H} also leads to a decrease in the Silk damping, thus increasing the temperature variance at large ℓ relative to the first peak. However, unlike “X”, Quintessence may also significantly reduce the conformal angular diameter distance to last scattering thus partially mitigating the shift in the location of the first CMB peak [50]. For the AS potential, this is not expected to be a large effect because the field becomes trapped in its minimum at $z \sim z_\Lambda$ which, for $\Omega_Q^{(RD)} \lesssim 0.1$, is above $z_\Lambda \gtrsim 16$. Another major difference between “X” and “Q” is the absence of clustering on subhorizon scales, hence there is no enhanced early ISW effect for Quintessence. But there is an ISW effect for this potential [52] because of the dramatic decrease in ρ_Q as the minimum of the Quintessence potential is

approached before $\sim z_\Lambda$. This results in an intermediate-to-late ISW effect reducing all the peak amplitudes in the power spectrum because the COBE normalization fixes the amplitude of the power spectrum at large scales.

“G”

Here, once again, there are two different approaches to perturbations in the field depending upon the preference for unmodified forms of the geometric/gravitational quantities or for unmodified stress-energy terms. As before, we adopt the latter approach. From this vantage point the perturbations in the energy density, pressure, and velocity divergence are the same as in equations (39), (40), and (41), but the Klein-Gordon equation for the perturbations now assumes the form

$$\begin{aligned} \delta\ddot{\phi} + 2\mathcal{H}\delta\dot{\phi} + (k^2 + a^2\bar{V}_{\phi\phi})\delta\phi - \bar{\phi}\dot{\delta}_C &= \frac{a^2}{2} [\bar{F}_\phi\delta R + \bar{F}_{\phi\phi}\bar{R}\delta\phi] \\ &= \frac{a^2\bar{R}}{2\bar{E}} \left[\bar{F}_{\phi\phi} - \frac{\bar{F}_\phi^2}{\bar{F}} - \frac{3\bar{F}_\phi^2\bar{F}_{\phi\phi}}{2\bar{F}} \right] \delta\phi + \frac{a^2\bar{F}_\phi}{2\bar{F}\bar{E}} \left[\delta\rho - 3\delta P + 3(\bar{F}_\phi\bar{V}_{\phi\phi} + \bar{F}_{\phi\phi}\bar{V}_\phi)\delta\phi - \frac{6\bar{F}_{\phi\phi}\bar{\phi}\delta\dot{\phi}}{a^2} \right] \end{aligned} \quad (47)$$

and we have dropped the $F_{\phi\phi\phi}$ term. Note that for this potential and coupling

$$\begin{aligned} 3(\bar{F}_\phi\bar{V}_{\phi\phi} + \bar{F}_{\phi\phi}\bar{V}_\phi)\delta\phi - \frac{6\bar{F}_{\phi\phi}\bar{\phi}\delta\dot{\phi}}{a^2} \\ = -3\xi(1+\alpha)\delta\rho_G - 3\xi(1-\alpha)\delta P_G. \end{aligned} \quad (48)$$

The minimally-coupled limit of this model is another frequently studied quintessence potential [54, 56, 57]. This potential is in some respects the opposite of the Albrecht-Skordis model where the energy density during the early Universe can be considerable and may lead to a swifter expansion prior to its entrapment at z_Λ . In contrast, for the Inverse Power Law potential the opposite occurs: the Quintessence energy density is inconsequential during much of the evolution of the Universe, only becoming important as the present epoch is approached.

In the minimal-coupling limit the superhorizon perturbations during the radiation dominated epoch may be derived in the usual way, leading to

$$\delta_G = \frac{4\alpha}{3(5\alpha+26)}\delta_C \quad (49)$$

$$\frac{\delta\phi}{\bar{\phi}} = \frac{4}{5\alpha+26}\delta_C \quad \frac{\delta\dot{\phi}}{\dot{\bar{\phi}}} = \frac{8+2\alpha}{5\alpha+26}\delta_C \quad (50)$$

with no change in δ_C . Note that when $\alpha \rightarrow \infty$ we regain the results of the exponential potential (see equation (43)) and, when $\alpha = 0$, the vacuum result $\delta_\Lambda = 0$.

Again, on superhorizon scales there is no change in the evolution of δ_C during either matter or radiation domination and similarly, on subhorizon scales, the Quintessence perturbations decay [6, 54] but unlike “Q” there is no suppression in the growth of matter perturbations. The negligible Quintessence energy density also means that there is no change in the size of the sound horizon at recombination. There is, however, a significant decrease in the angular diameter distance because of the contribution from the Quintessence energy density at low redshifts that causes a shift in the peak positions to smaller ℓ and decreases their separation. This effect increases with α because the equation of state and, thus, the energy density ρ_G are correlated with the exponent: smaller α correspond to smaller ρ_G at a fixed redshift. The peak heights are suppressed relative to the COBE normalization point because the larger Quintessence energy density terminates matter domination at an earlier epoch. This enhances the late ISW effect, increasing the variance on large scales and therefore lowering the initial amplitude of the power spectrum. Once again, this effect increases with α for exactly the same reason.

For the non-minimally coupled case, $\xi \neq 0$, the situation is much more complex. All the effects discussed above for the minimally-coupled limit apply but now we must also take into account the change in F . A reduction in the strength of gravity, $F \geq 1$, now slows the expansion, leading to a larger sound horizon at recombination. If F remained constant there would be a compensating

change in the distance to the last scattering surface and the peak positions would be unaffected. However F must decrease in order to attain $F = 1$ at the present time, so this distance can only be smaller than that required to leave the peak positions unaltered. Hence a decrease in G shifts the CMB anisotropy spectrum peaks to even smaller ℓ . The changing F also reduces the ratio of the amplitude of the first peak to the others by partially cancelling the early ISW effect. Simultaneously, the decrease in \mathcal{H} shifts the peaks to larger scales due to the fact that thermal contact between the baryon-photon fluid can be maintained down to a lower the redshift. The slower expansion also increases the duration of recombination leading to more effective photon diffusion, decreasing the temperature variance on small scales.

VI. CONSTRAINTS FROM THE CMB

Unlike their similarities for BBN, the three cases we are considering here, extra relativistic energy density (“ X ”), a minimally coupled scalar field (“ Q ”), and a non-minimally coupled scalar field (“ G ”), all influence the formation of the CMB anisotropy spectrum differently, albeit with some features in common. To explore the CMB constraints we use modified versions of CMBFAST [58] to construct the anisotropy spectra and vary ΔN_ν and the baryon density parameter η_{10} . We compare the models to the data from the BOOMERANG [59], MAXIMA [60], and DASI [61] detectors, employing RADPACK [62] to determine the goodness of fit and we assign the confidence level based on $\Delta\chi^2$. RADPACK also allows us to adjust the calibration of each data set, at the cost of a χ^2 penalty. The current data covers the first three peaks in the \mathcal{C}_ℓ with reasonable accuracy, so while subtle effects may be missed, this approach is sufficient to extract the gross features of each model. Since here we are concentrating on constraints in the $\Delta N_\nu - \eta$ plane, we have limited the priors, adopting those of the “concordance Λ CDM” model: $\Omega_{\text{tot}} = 1$, $\Omega_M = 0.3$, $H_0 = 72 \text{ kms}^{-1}\text{Mpc}^{-1}$, along with no “tilt” ($n = 1$). As in related, earlier work (see, *e.g.*, [63, 64, 65, 66]) here we explore the constraints on ΔN_ν derived from the CMB anisotropy.

Because the CMB constraints in the non-minimally coupled case “ G ” differ from those for “ X ” and “ Q ” we discuss this case, G , separately. We note here that Chen and Kamionkowski [71] have discussed how constraints from the CMB may be used to provide a test of Brans-Dicke cosmology, which bears some relation to our case “ G ”.

First, we consider “ X ”. In general, there is an intimate interplay between η_{10} and ΔN_ν^X as shown by the solid curves in Figure 4 where our results reveal that an *increase* in ΔN_ν can, to some extent, be compensated by a *reduction* in η . This degeneracy is the result of similar effects upon the relative heights of the first and second peak and is only broken by the presence of the third peak

in the spectrum. Increasing ΔN_ν^X leads to a larger early ISW effect boosting the variance at the first peak relative to the rest, while increasing η_{10} changes the relative heights of the odd and even peaks. At the same time increasing ΔN_ν^X reduces the sound horizon by reducing the conformal age of the Universe at last scattering, but the presence of $\bar{\rho}_B$ in equation (38) reveals that a reduction in η_{10} can compensate this change by increasing the baryon-photon sound speed which overwhelms the simultaneous increase in redshift at which recombination occurs.

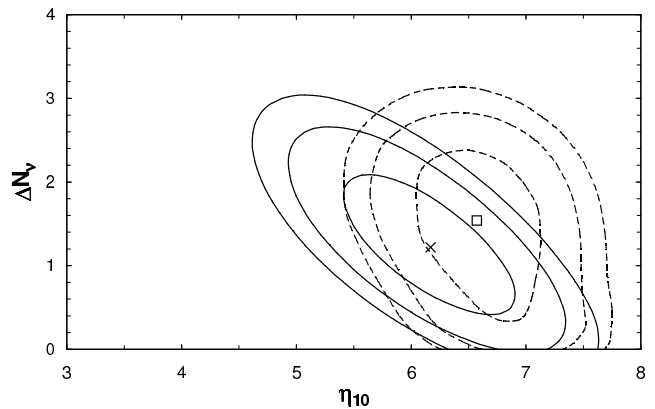


FIG. 4: CMB likelihood contours, 68%, 95%, and 99%, for “ X ” (solid) and “ Q ” (dashed). The best fit points are indicated by the cross for “ X ”, and by the square for “ Q ”.

The dotted curves in Figure 4 show the contours for “ Q ”. In this case they lack the strong anticorrelation between ΔN_ν and η that “ X ” exhibited. Despite the differences between “ X ” and “ Q ”, the bounds from the CMB are quite similar in both cases, with best fit values of $\eta_{10} \approx 6.2 - 6.5$ ($\Omega_B h^2 \approx 0.023 - 0.024$) and non-zero $\Delta N_\nu \approx 1.2 - 1.6$, while the 99% upper bound to ΔN_ν in both cases is $\Delta N_\nu \lesssim 3.2$ ($\Omega_Q^{(RD)} \lesssim 0.34$, $\lambda \gtrsim 3.4$).

For comparison with the CMB fluctuation data, the case of non-minimally coupled fields has several unique features which distinguish it from the other two cases considered above. The confidence contours shown in Figure 5 compare the results for two choices of α . A comparison of Figures 4 & 5 reveals that the anticorrelation between η_{10} and ΔN_ν^G is very strong for the non-minimally coupled case G , with the centroid of the contours dependent on α as is the elongation of the contours. We also note that the χ^2 at the best fit point decreases with α *i.e.*, $\alpha = 2$ is a better fit than $\alpha = 4$ and $\alpha = 1$ is a better fit than $\alpha = 2$. The large shift in and the sensitivity of η_{10} to α can be understood as follows. Inverse Power Law potential models generically *reduce* the heights of all the peaks because of the late ISW effect and this suppression decreases with α . The peak suppression favors shifts in the experimental calibrations, so by increasing the baryon to photon ratio there is a deflection of some

of the χ^2 penalty by improving the fit to the first and third peaks at the expense of making the fit to the second peak worse. Additionally raising η_{10} suppresses the Silk damping boosting the temperature variance at large ℓ relative to that at the first peak. Lastly, as we noted before for “X”, raising η_{10} will also reduce the sound horizon at last scattering which will compensate for the reduction of the angular diameter distance in these models. The shift in the centroid of the contours is due to the reduction of the strength of the late ISW effect as α decreases since the increase in η_{10} needed to raise the peak amplitudes becomes smaller. The anticorrelation of η_{10} and ΔN_ν^G is largely the result of the change in the early ISW effect. As ΔN_ν^G increases the ratio of the first to second peak amplitudes also increases which, like ΔN_ν^X , can be compensated by reducing η_{10} .

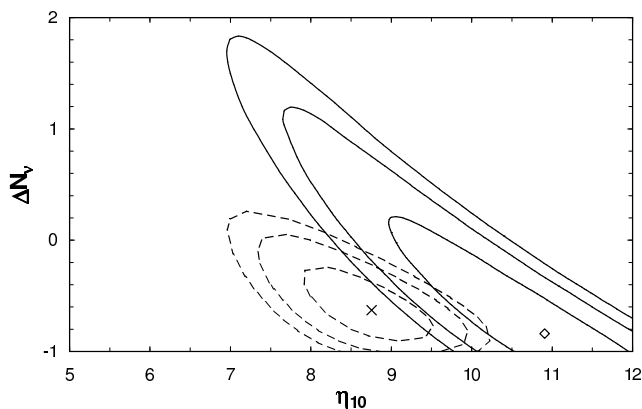


FIG. 5: CMB likelihood contours, 68%, 95%, and 99%, for “G” and two values of α , the IPL exponent. The solid contours are for $\alpha = 4$ and the dashed contours are for $\alpha = 1$. The best fit points are indicated by the diamond for $\alpha = 4$ and the cross for $\alpha = 1$.

Clearly, in this case the best fit values and the bounds for η_{10} and ΔN_ν^G are functions of α . For $\alpha = 4$ we have $\eta_{10} = 10.9$, $\Delta N_\nu^G = -0.84$ with a 99% upper bound of $\Delta N_\nu^G \lesssim 1.8$, for $\alpha = 2$ we find $\eta_{10} = 10.0$, $\Delta N_\nu^G = -0.90$ with a 99% upper bound of $\Delta N_\nu^G \lesssim 0.2$ while for $\alpha = 1$ we find $\eta_{10} = 8.8$, $\Delta N_\nu^G = -0.63$ with a 99% upper bound of $\Delta N_\nu^G \lesssim 0.3$. However, as we mentioned earlier, the χ^2 at the minima for $\alpha = 4$ is large (130 for 39 degrees of freedom) and we can rule out this model as incompatible with the data at an extremely high confidence level (formally, at $\sim 10^{-11}$). The case of $\alpha = 2$ is only marginally CMB-compatible, at the 99% confidence level, while the $\alpha = 1$ model is perfectly acceptable. These results are in agreement with previous studies on limits to α : Malquarti and Liddle [67] find $\alpha < 2$ at 95% in the minimal limit while Bean & Melchiorri [68], Hannestad & Mörtsell [69] and Melchiorri *et al.* [70], have found that the effective equation of state for Quintessence must be close to -1 which imposes a similar constraint on α [19].

As in our discussion of BBN, we must discuss some caveats to our CMB results. When $\Delta N_\nu^X > 0$, the enhanced *relativistic* energy density keeps the early universe radiation-dominated to a lower redshift. To some extent this can be compensated by an increase in the *matter* density Ω_M . However, since in our CMB fits we have fixed Ω_M at 0.3, the ranges of ΔN_ν^X shown in Figure 4 are overly restrictive (compare, *e.g.*, with [66]). However, this bias will be ameliorated in the combined BBN – CMB likelihood distributions since, as may be seen by comparing Figures 3 and 4, the dominant constraint on ΔN_ν^X is provided by BBN. We must again point out that the solar system limits to G' will further restrict the allowed range of ΔN_ν^G and indeed the best fit points shown in Figure 5 are all outside of the allowed range corresponding to the bounds in G in eq. (19). For non-minimally coupled scalar fields the upper and lower bounds to ΔN_ν^G are functions of the Inverse Power Law exponent α in the adopted scalar field potential.

VII. COMBINING BBN AND CMB

For a self-consistent cosmology any modifications to SBBN at redshift $\sim 10^{10}$ must be consistent with those deviations from the standard-model predictions for the later evolution of the universe as probed by the CMB ($10^4 \gtrsim z \gtrsim 0$). While BBN and the CMB favor slightly different regions in the $\Delta N_\nu - \eta$ plane, there is, indeed, overlap for models with new particles (“X”) and for those with minimally-coupled scalar fields (“Q”). In Figure 6 are shown the joint BBN-CMB likelihood contours for these two cases. Although the best fits do occur for small, nonzero values of ΔN_ν ($\Delta N_\nu \approx 0.1$, $\eta_{10} \approx 6.6 \iff \Omega_B h^2 \approx 0.024$), the deviation from $\Delta N_\nu = 0$ is not statistically significant and the “standard” model ($\Delta N_\nu = 0$) is entirely consistent with the BBN and CMB data. For both “X” and “Q”, the minimum χ^2 in our combined BBN – CMB fit is 47 for 39 degrees of freedom; for these cases there is consistency between the models and the universe at $z \approx 10^{10}$ and at $z \approx 0$.

In top panel of Figure 7 are shown the joint BBN-CMB likelihood contours for the “G” case, but only for $\alpha = 1$: we do not show likelihood contours for the other two α values since these models ($\alpha = 2, 4$) are ruled out at better than 99% confidence. For $\alpha = 1$ the χ^2 at the minimum for the joint BBN-CMB fits is slightly larger than for “X” and “Q”, at 57 for 39 degrees of freedom; this non-minimally coupled model is compatible with the data at 97% confidence level. The minimum for this model occurs at $\Delta N_\nu^G \approx -0.51$, $\eta_{10} \approx 8.2$ ($\Omega_B h^2 \approx 0.030$), with a significant autocorrelation between the two quantities. The deviation from $\Delta N_\nu = 0$ is now rather large: the minimum along $\Delta N_\nu = 0$ is located on the 90% confidence contour.

Finally in the bottom panel of Figure 7 we impose the limits to G' we have mentioned so frequently. The minimum from the top panel is outside the allowed region

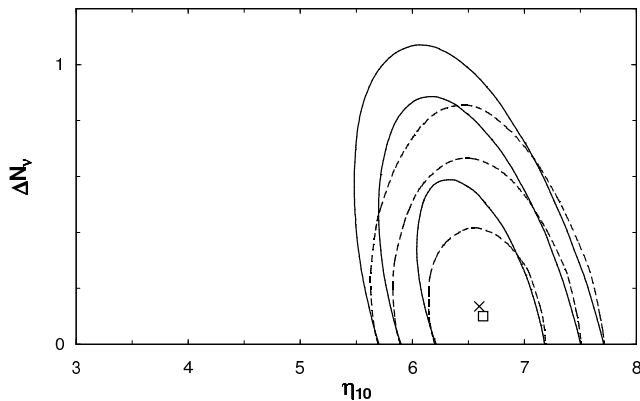


FIG. 6: Joint BBN and CMB likelihood contours, 68%, 95%, and 99%, for “X” (solid) and “Q” (dashed). The best fit points are indicated by the cross for “X” and by the square for “Q”.

$\Delta N_\nu^G = \pm 0.15$ and now resides on the boundary at $\Delta N_\nu^G \approx -0.15$, $\eta_{10} \approx 7.6$ ($\Omega_B h^2 \approx 0.028$). The χ^2 at the minimum is such that the goodness-of-fit of the model is only compatible with the data at the 98% level.

VIII. SUMMARY

BBN and the CMB provide complementary constraints on models for the dark matter/energy at completely distinct epochs in the evolution of the universe. Consistency with both sets of constraints can help in distinguishing among different models for new physics beyond the standard models of cosmology and particle physics. As discussed here, models with extra particles which are relativistic during the early evolution of the universe (“X”) and those with minimally-coupled scalar fields (“Q”) yield similar predictions for BBN ($\eta_{10} \approx 5.0$ and $\Delta N_\nu \approx 0$; see §III, especially Figs. 1 & 3) and for the CMB ($\eta_{10} \approx 6.2-6.5$ and $\Delta N_\nu \approx 1.2-1.6$; see §VI and Fig. 4). As a result, they also provide similar good fits to the joint BBN-CMB constraints (see §VII and Fig. 6) with the baryon density being largely determined by the CMB constraints and ΔN_ν by BBN. While the best fits to the data for these two options are in fact compatible with $\Delta N_\nu = 0$ (at $\Omega_B h^2 \approx 0.024$ in both cases), some dark energy is permitted: at 99% confidence level $\Delta N_\nu^X \lesssim 1.07$ while $\Delta N_\nu^Q \lesssim 0.85$ ($\Omega_Q^{(RD)} \lesssim 0.12$, $\lambda \gtrsim 5.7$). In contrast, the new physics associated with non-minimally coupled scalar fields (“G”) induces some unique behavior, leading to quite different BBN and CMB constraints which, in general, are quite difficult to satisfy simultaneously. Because such models generally modify the strength of gravity during the earlier evolution of the universe, $\Delta N_\nu^G < 0$ is not only allowed, it is favored by both the BBN and CMB constraints (see §III, especially Fig. 2 and §VI, es-

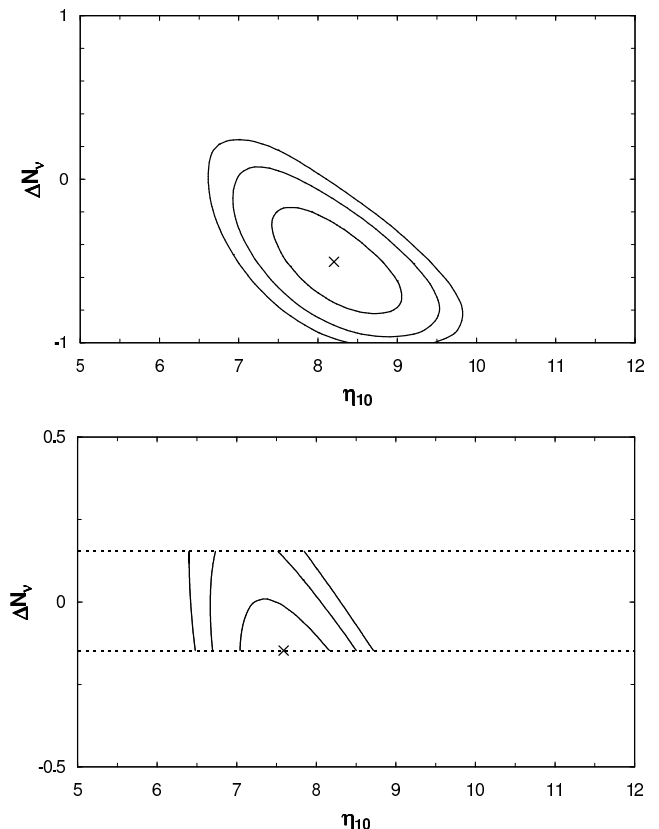


FIG. 7: Joint BBN and CMB likelihood contours, 68%, 95%, and 99%, for “G”, $\alpha = 1$. The top panel is with no G constraints eq. (19), the bottom is with those constraints. The best fit points are indicated by the crosses.

pecially Fig. 5). However, for “G” the allowed regions in the $\Delta N_\nu - \eta$ plane are sensitive to the form of the scalar field potential (see Fig. 5). For inverse power law potentials, only those models with $\alpha \lesssim 1$ have CMB-identified regions which have significant overlap with the regions compatible with the BBN constraints (compare Figs. 2 & 5). Furthermore, since there are solar system constraints on the possible variation of G , there are non-BBN and non-CMB constraints on G'/G (see eq. (19)) which provide independent constraints on ΔN_ν^G . When these are combined (for $\alpha = 1$) with the BBN and CMB constraints the best fit value of ΔN_ν^G is at -0.15 and $\Omega_B h^2 \approx 0.028$ (see Fig. 7). However, we note that there is less than a 2% probability that this model is, in fact, compatible with the current BBN and CMB data.

The two models for Quintessence we have investigated in this paper are by no means the only plausible examples of dynamic dark energy. What distinguishes the two cases we have considered is their importance during BBN and their role in the generation of the primary anisotropies in the CMB. In fact, in this regard, these two models are unique since it is much more common for

Quintessence models to become important only at low redshifts. In such cases BBN provides few, if any, constraints and the primary anisotropies of the CMB are unaffected. The influence of the dark energy is via the change in redshift of matter-dark energy equality and thus the corresponding COBE normalization of the matter power spectrum. For the CMB this translates into a global stretching of the peaks in the spectrum and a reduction in their amplitudes but for Large (and Small) Scale Structure (LSS), Type Ia supernovae observations, and weak lensing surveys the change in the extent of matter perturbation growth is more important and their observation will provide valuable additional and complimentary constraints upon the models [72, 73, 74]. The minimally coupled IPL potential falls into this category. The CMB already constrains $\alpha < 2$ [67] and including LSS and Type Ia supernova data yields $w_G \lesssim -0.7$ at the present time which translates into $\alpha < 1.5$ for the concordance model values of H_0 and Ω_M .

These same cosmological tests also furnish constraints upon the two models we have examined: “Q” and “G”. For the pure exponential potential these signatures were discussed by Ferreira & Joyce [6] and the Albrecht Skordis modification (our case “Q”) by Skordis & Albrecht

[52]. In contrast with typical Quintessence models the AS potential modifies the matter power spectrum mainly by inhibiting the growth of density perturbations rather than changing the COBE normalization. The essentially stationary field below the redshift of $z_\Lambda \gtrsim 15$ (corresponding to $\lambda \gtrsim 5.7$) leads to little change in the magnitude-redshift relation that could be probed by Type Ia supernovae. For the non-minimally coupled Inverse Power Law model the effects are supplementary to those in the minimal limit. A non-zero ξ will introduce additional effects through the change in gravitational strength F that in turn will alter the growth of density perturbations by directly influencing their growth in addition to the change in the normalization.

Acknowledgments

For valuable discussions and advice we wish to thank R. Scherrer, M. Kaplinghat, X.Chen and A. Zentner. We acknowledge the support of the DOE through grant DE-FG02-91ER40690.

-
- [1] I. Zlatev, L. Wang, & P. J. Steinhardt, Phys. Rev. Lett. **82**, 896 (1999).
 - [2] J. Frieman & I. Waga, Phys. Rev. **D57**, 4642, (1998).
 - [3] P. J. Steinhardt, L. Wang & I. Zlatev, Phys. Rev. **D59**, 123504, (1999).
 - [4] S. A. Bludman & M. Roos, Phys. Rev. **D65**, 43503, (2002).
 - [5] A. R. Liddle & R. J. Scherrer, Phys. Rev. **D59**, 023509, (1999).
 - [6] P. G. Ferreira & M. Joyce, Phys. Rev. **D58**, 023503, (1998).
 - [7] E. J. Copeland, A. R. Liddle & D. Wands, Phys. Rev. **D57**, 4684, (1998).
 - [8] A. Albrecht & C. Skordis, Phys. Rev. Lett. **84**, 2076, (2000).
 - [9] S. Dodelson, M. Kaplinghat & E. Stewart, PRL, **85**, 5276, (2000).
 - [10] S. Hanany *et al.*, ApJ **545**, L1 (2000).
 - [11] J.-C. Hwang, ApJ, **375**, 443, (1991).
 - [12] J.-C. Hwang, Phys. Rev. **D53**, 762, (1996).
 - [13] J.-C. Hwang & H. Noh, Phys. Rev. **D54**, 1460, (1996).
 - [14] X. Chen, R. J. Scherrer, & G. Steigman, Phys. Rev. **D63**, 123504 (2001).
 - [15] C. Baccigalupi, S. Matarrese, & F. Perrota, Phys. Rev. **D62**, 123510 (2000).
 - [16] F. Perrota, C. Baccigalupi, & S. Matarrese, Phys. Rev. **D61**, 023507 (2000).
 - [17] S. M. Carroll & M. Kaplinghat, Phys. Rev. **D65**, 063507, (2002)
 - [18] J. P. Uzan, Phys. Rev. **D59**, 123510, (1999).
 - [19] L. Strigari & J. P. Kneller, in preparation, (2002).
 - [20] G. Steigman, D. N. Schramm, & J. E. Gunn, Phys. Lett. **66B**, 202 (1977).
 - [21] R. Epstein, J. Lattimer, & D. N. Schramm, Nature **263**, 198 (1976).
 - [22] S. Burles & D. Tytler, ApJ **499**, 699 (1998a).
 - [23] S. Burles & D. Tytler, ApJ **507**, 732 (1998b).
 - [24] J. M. O’Meara, *et al.*, ApJ **552**, 718 (2001).
 - [25] M. Pettini & D. V. Bowen, ApJ **560**, 41 (2001).
 - [26] S. D’Odorico, M. Dessauges-Zavadsky, & P. Molaro, A&A **338**, L1 (2001).
 - [27] G. Steigman, To appear in the Proceedings of the STScI Symposium, “The Dark Universe: Matter, Energy, and Gravity” (April 2 – 5, 2001), ed. M. Livio (astro-ph/0107222).
 - [28] S. A. Levshakov, M. Dessauges-Zavadsky, S. D’Odorico, & P. Molaro, ApJ **565** 696 (2002).
 - [29] S. A. Levshakov, W. H. Kegel & F. Takahara, ApJ **499**, L1 (1998).
 - [30] S. A. Levshakov, W. H. Kegel & F. Takahara, A&A **336**, 29L (1998).
 - [31] S. A. Levshakov, W. H. Kegel & F. Takahara, MNRAS **302**, 707 (1999).
 - [32] Y. I. Izotov, T. X. Thuan, & V. A. Lipovetsky, ApJS **108**, 1 (1997).
 - [33] Y. I. Izotov & T. X. Thuan, ApJ **500**, 188 (1998).
 - [34] K. A. Olive & G. Steigman, ApJS **97**, 49 (1995).
 - [35] K. A. Olive, E. Skillman, & G. Steigman, ApJ **483**, 788 (1997).
 - [36] B.D. Fields & K. A. Olive, ApJ **506**, 177 (1998).
 - [37] M. Peimbert, A. Peimbert, & M. T. Ruiz, ApJ **541**, 688 (2000).
 - [38] R. Gruenwald, G. Steigman, & S. M. Viegas, ApJ **567**, 931 (2002).
 - [39] S. M. Viegas, R. Gruenwald, & G. Steigman, ApJ **531**, 813 (2000).

- [40] D. Sauer & K. Jedamzik, *A&A* **381**, 361 (2002).
- [41] K. A. Olive, G. Steigman, & T. P. Walker, *Phys. Rep.* **333**, 389 (2000).
- [42] L. Randall & R. Sundrum, *Phys. Rev. Lett.* **83**, 4690 (1999).
- [43] J. Bratt, A. C. Gault, R. J. Scherrer, & T. P. Walker, *astro-ph/0208133* (2002).
- [44] R. Bean, S. H. Hansen, & A. Melchiorri, *Phys. Rev.* **D64**, 103508 (2001).
- [45] C.-P. Ma & E. Bertschinger, *ApJ*, **455**, 7, (1995).
- [46] W. Hu & N. Sugiyama, *Phys. Rev.* **D51**, 2599, (1995).
- [47] J.-C. Hwang, *ApJ*, **415**, 486, (1993).
- [48] J. Silk, *ApJ*, **151**, 459, (1968).
- [49] W. Hu, M. Fukugita, M. Zaldarriaga & M. Tegmark, *ApJ*, **549**, 669, (2000).
- [50] M. Doran, M. Lilley, J. Schwindt & C. Wetterich, *ApJ*, **559**, 501, (2001).
- [51] W. Hu, D. Scott, N. Sugiyama & M. White, *Phys. Rev.* **D52**, 5498, (1995).
- [52] C. Skordis & A. Albrecht, Submitted to *Phys. Rev. D*, (2000).
- [53] W. Hu, *ApJ*, **506**, 485, (1998).
- [54] B. Ratra & P. J. E. Peebles, *Phys. Rev.* **D37**, 3406, (1988).
- [55] R. Dave, R. R. Caldwell & P. J. Steinhardt, *astro-ph/0206372*, (2002).
- [56] C. Baccigalupi, A. Balbi, S. Matarrese, F. Perrotta & N. Vittorio, *Phys. Rev.* **D65**, 063520 (2002).
- [57] M. Yahiro, G. J. Mathews, K. Ichiki, T. Kajino & M. Orito, *Phys. Rev.* **D65**, 063502 (2002).
- [58] U. Seljak & M. Zaldarriaga, *ApJ*, **469**, 437 (1996).
- [59] C. B. Netterfield, *et al.*, *ApJ* **571**, 1 (2002).
- [60] A. T. Lee, *et al.*, *ApJ* **561**, L1 (2001).
- [61] N. W. Halverson, *et al.*, *ApJ* **568**, 38 (2002).
- [62] J. R. Bond, A. H. Jaffe, & L. Knox, *ApJ*, **533**, 19 (2000).
- [63] J. Lesgourgues & M. Peloso, *Phys. Rev.* **D62**, 081301 (2000).
- [64] S. Hannestad, *Phys. Rev. Lett.* **85**, 4203 (2000).
- [65] S. Esposito, G. Mangano, A. Melchiorri, G. Miele, & O. Pisanti, *Phys. Rev.* **D63**, 043004 (2001).
- [66] J. P. Kneller, R. J. Scherrer, G. Steigman, & T. P. Walker, *Phys. Rev.* **D64**, 123506 (2001).
- [67] M. Malquarti & A.R. Liddle, *astro-ph/0203232* (2002).
- [68] R. Bean & A. Melchiorri, *Phys. Rev.* **D65**, 041302 (2001)
- [69] S. Hannestad & Mörtsell, *Phys. Rev.* **D66**, 063508, (2002).
- [70] A. Melchiorri, *et al.*, *astro-ph/0211522*
- [71] X. Chen & M. Kamionkowski, *Phys. Rev.* **D60**, 104036 (1999)
- [72] M. Bartelmann, F. Perrotta & C. Baccigalupi, *A&A*, **396**, 21 (2002)
- [73] K. Benabed & F. Bernardeau, *Phys. Rev.* **D64**, 083501 (2001)
- [74] D. Huterer, *Phys. Rev.* **D65**, 063001 (2002)
- [75] Except during phases when the number of degrees of freedom is changing such as when a massive particle species decays or annihilates.
- [76] The equality of the equations of state is temporarily violated, at the $\sim 10\%$ level, during the transition from a radiation dominated to a matter dominated fluid.
- [77] The radiation/matter transition causes a slight deviation from this formula at the $\sim 5\%$ level.
- [78] This confirms our previous statement concerning that $w_Q \rightarrow w_f$ in the limit $\alpha \rightarrow \infty$.
- [79] There is an exception provided by the type II Randall-Sundrum model [42] which modifies the Friedmann equation through the addition of two extra terms, one of which behaves exactly like “radiation” ($w = 1/3$) but whose sign may be positive or negative. For a recent analysis of the constraints on such models and for further references, see [43]